Journal of the Chinese Society of Mechanical Engineers, Vol.47, No.1, pp35~47 (2026)

Effect of Surface Roughness and Texture Arrangements on the Performance of Composite Micro-Texture Journal Bearing

Lili Wang*, Min Wang**, Jingdong Duan***, Wei Zhang*** and Ying'ao Liu***

Keywords: composite micro-texture journal bearing, static and dynamic characteristics, surface roughness, texture arrangement, texture distribution position

ABSTRACT

To improve the loading capacity, antifriction performance, and the dynamic characteristics of journal bearing, the composite micro-texture journal bearing is studied, the influence of surface roughness and texture arrangements on the micro-textured bearing is further considered. The surface roughness model, the oil film thickness equation of composite micro-texture, the generalized Reynolds equation of journal bearings, the dynamic characteristics calculation model of micro-textured bearing rotor system is established. The static and dynamic characteristics of bearing with different distribution position, arranges of composite micro texture considering surface roughness are studied. The results show that the proper roughness can improve the lubrication performance of bearing, and the lubrication performance is better when the roughness value is 0.209μm. The composite micro-texture is distributed around 160 °, and the triangular composite diamond micro-texture bearing has good stability and lubrication performance. When the micro-textures arrange in parallel along the circumference considering surface roughness, better static and dynamic characteristics are gained.

Paper Received July, 2024. Revised March, 2025. Accepted March, 2025. Author for Correspondence: Lili Wang, Min Wang.

* *Associate Professor, College of Mechanical and Electronic Engineering, Shandong University of Science and Technology, Qingdao, China 266590.*

** *Associate Professor, College of Mechanical and Electronic Engineering, China university of Petroleum, Qingdao, China 266580.*

*** *Graduate Student, College of Mechanical and Electronic Engineering, Shandong University of Science and Technology, Qingdao, China 266590.*

INTRODUCTION

With the development of mechanical equipment to high-precision, extreme and compound direction, the requirement for the stability and lubrication performance of journal bearings is increasing. In the traditional bearing performance analysis, the journal and bearing bush are mostly regarded as the smooth surfaces. In the practice, the surface of parts obtained by any processing method is not smooth, and different processing technologies will result in different roughness of processing surface (Zhang et al, 2017). Gururajan et al. (Gururajan& Prakash,2000) and Singh (Singh, 2020) established the mathematical model of bearing considering surface roughness, pointed that there was a big difference between considering roughness and ignoring roughness. Through the dynamic trajectory analysis of the rotor supported by two radial bearings, Chang (Chang&Cai, 2013) concluded that the difference of the dynamic response between considering and not considering the effect of roughness was obvious. Narwat et al. (Narwat 2023) considered the bearing with micro-roughness and reported that transverse roughness can improve bearing performance indices. Pham-Ba et al. (Son& Molinari, 2021) found that the surface roughness will develop towards a common stable state under the condition of non-lubricated wear, within a certain range of load conditions. Kumarab et al. (Kumarab &Azama, 2021) described the performance of Rayleigh stepped bearings under the mixed elastohydrodynamic lubrication with the directional random roughness, the results showed that greater pressure generated in the contact area of bearings with the roughness of transverse orientation. Cheng et al. (Cheng et al, 2024) showed that the effect of surface morphology is crucial as the mixed lubrication regime under start-stop or heavy load conditions. Li et al. (Li&An, 2019) established a calculation model of thrust journal bearing considering the roughness, showed that with the reduction of surface roughness, oil film pressure, vertical acceleration and additional load decreased. Maharshi et al. (Maharshi et al, 2018) solved the Reynolds equation with random parameters

(eccentricity and surface roughness), showed that randomness had a significant impact on bearing performance. The results of the above researchers show that the bearing performance considering the roughness will be closer to the actual operating conditions of the bearing, and can significantly improve the lubrication performance of the bearing and reduce the friction coefficient.

At the same time, the research in the recent years shows that machining micro texture on the surface of the bearing bush can also improve the bearing capacity and reduce the wear (Zhou et al, 2021). Zhang et al. (Zhang et al 2019) summarized the mechanism of surface micro-texture technology to improve the tribological characteristics of friction pairs. Kumar et al. (Kumar &Sharma, 2019) studied the influence of surface texture on the static and dynamic characteristics of thrust bearing, showed that machining micro-texture on the bearing surface can significantly improve the bearing capacity, stiffness coefficient and reduce friction power loss. Profito et al. (Profito et al, 2024) investigated the friction reduction mechanisms of textured journal bearings. Vidyasagar et al. (Vidyasagar et al, 2021) used nanosecond fiber laser to fabricate snakeskin texture on the inner ring of FAG radial ball bearing. Obilor et al. (Obilor et al, 2022) reviewed the recent progress of polymer laser ablation, and provided a systematic summary and guidance for future micro-texture processing technology. Wang et al. (Wang et al,2019) showed that reasonable selection of micro-texture distribution position, depth and coverage can effectively reduce the friction of friction pair. Atwal et al. (Atwal &Pandey, 2021) showed that the friction coefficient of the bearing with the composite of rectangular and fish scale micro-texture reduced significantly. Pattnayak et al. (Pattnayak et al, 2022) designed a micro-texture similar to the skin of freshwater fish, the static and dynamic performance of the rectangular composite biomimetic micro-texture bearing improved compared with the traditional micro-texture. Manser et al. (Manser, 2020) used the micropolar fluid model to study the combined effect of bearing surface texture and non-Newtonian fluid on the static characteristics of finite-length hydrodynamic radial journal bearings. Tauviqirrahman et al. (Tauviqirrahman et al, 2022) obtained an optimal locally textured radial plain bearing combined with a hydrophobic coating. Huang et al. (Huang et al, 2022) prepared AS-SnAgCu-TiC composite by filling the surface biomimetic texture of AS with multiple solid lubricants. Meng et al. (Meng et al, 2020) used ultrasonic surface rolling technology to prepare reinforced surface and line-textured surface on the substrate. Hua et al. (Hua et al, 2020) used the fiber laser to carry out the laser texture processing on the surface of GCr15 bearing steel, and prepared the spherical convex texture. Wang et al. (Wang et al, 2022) used a femtosecond laser to fabricate microgrooves on a steel substrate, and then deposited the superhydrophobic coatings in the microgrooves. Niu et al. (Niu et al, 2021) prepared the micro-textures with different parameters on the surface of medium carbon steel. Wang et al. (Wang et al, 2022) designed a textured surface on the friction pair, and the experimental results showed that the wear can be reduced by about 62.6% using the ellipsoid dimpled micro-textured surface. Chen et al. (Chen et al, 2018) established four numerical models of cylindrical micro-textures, both theoretical and experimental results showed that micro-textures had a good friction-reducing effect on piston rings. Dobrica et al. (Dobrica et al, 2009) presented that inertia effect affected the pressure in textured sliders.

Micro-texture can improve the lubricating performance of journal bearings. In order to obtain the best composite micro-texture with various shapes, and better improve the bearing lubrication performance, the influence of and composite micro-texture on bearing lubrication performance is studied. And in order to be more consistent with the actual processing conditions, the influence of surface roughness on the micro-textured bearing is further considered. By establishing a theoretical model of journal bearing considering surface roughness, changing the arrangement, distribution position of micro-texture in the bush, the best micro-texture arrangement, distribution position and shape are explored.

THEORETICAL MODELS

Structural model of composite micro-textured bearing

As shown in Figure 1, the two ends of the bearing are symmetrically supported by two identical journal bearings, assuming that the journal is parallel to the bearing pad and does not tilt. The parameters of journal bearings at both ends are the same, a hydrodynamic journal bearing is taken as an example to study the effect of composite micro-texture on the lubricating performance of the bearing. On the bearing surface, 30W fiber laser marking machine is used to process the micro texture. In the cross section of the radial bearing of Figure 1, φ_1~φ_2 are the micro-textured regions. θ is attitude angle, e is eccentricity, n is rotational speed, r is axis radius, R is bearing radius. The circumferential angle φ starts from the maximum oil film thickness h_{max}.

Figure 2 shows the expanded view of the composite micro-texture journal bearing in the circumferential direction. Many references show that

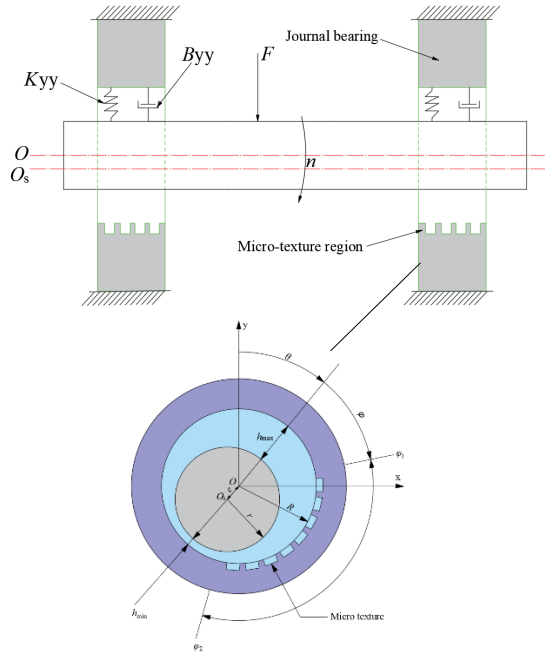

Fig. 1 Schematic diagram of bearing rotor system

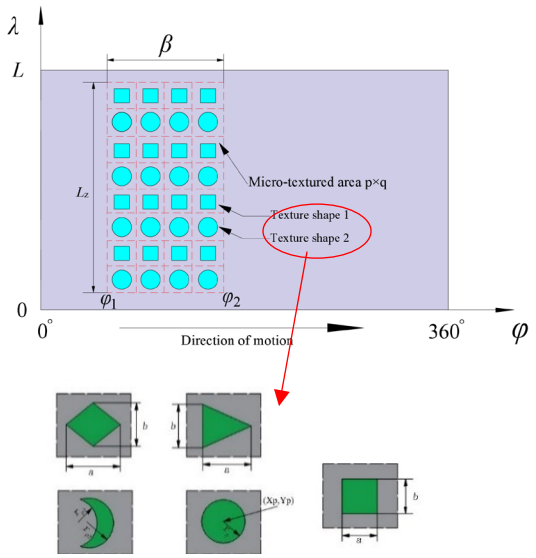

Fig.2 Diagram of journal bearing and micro-texture structure

the lubricating performance of journal bearings with full texture distribution reduces, while processing micro-textures in the divergent region of the oil film can have the positive effect. In the coordinate system, φ is the circumferential angle, and λ is the axial direction of the journal bearing. In the micro-texture distribution region, the total number of micro-textures is $p \times q$, of which p is the circumferential texture number and q is the axial texture number. The micro-texture structure adopts the more representative circular, crescent, hexagonal, rectangular, rhombus and triangular textures in the previous study (Zhao, 2020) and (Wang et al, 2023). By adjusting the radius of the micro-texture r_p, the size of the directional length b and the circumferential length a, the area of the micro-textures can be adjusted. Different shapes textures in the surface of friction pairs are combined to form different composite micro-textures, and Fig. 2 is one of the composite textures of circular and rectangular.

Control equations

Governing equations of oil film thickness considering surface roughness

The oil film thickness of the journal bearing is as following:

$$\begin{cases} h_1(x,y) = c_r + e\cos(\varphi-\theta) \\ h_2(x,y) = c_r + e\cos(\varphi-\theta) + \Delta h(x,y) \end{cases} \tag{1}$$

Where $h_1(x, y)$ is the oil film thickness without considering the micro texture, $h_2(x, y)$ is the oil film thickness considering the micro-texture, c_r is the radial clearance of the journal bearing, $\Delta h(x,y)$ is the texture depth.

In the composite micro-texture region, each micro-texture is called a micro-texture unit, and in the x, y coordinate system, each micro-texture center corresponds to the coordinate (x_p, y_p) as shown in Fig.2. In the texture region, oil film thickness need to be increased by Δh; for defining the texture region range, combined with the texture shape parameter a, b shown in Fig. 2 and geometric expression of shape, the texture region of the triangular composite rhombus micro-textures is characterized as follows:

$$\Delta h(x,y) = \begin{cases} h_{p1}, & -\frac{a}{2} \le (x-x_{p1}) \,\&\&\, \frac{b}{2a}(x-x_{p1}) + \frac{3b}{4} \le (y-y_{p1}) \le -\frac{b}{2a}(x-x_{p1}) - \frac{3b}{4} \\ h_{p2}, & -\frac{b}{a}(x-x_{p2}) - b \le (y-y_{p2}) \le \frac{b}{a}(x-x_{p2}) + b \,\&\&\, \frac{b}{a}(x-x_{p2}) - b \le (y-y_{p2}) \le -\frac{b}{a}(x-x_{p2}) + b \end{cases} \tag{2}$$

In a similar way to equation (2), the texture region of the rhombus composite fish-shaped micro-textures is characterized as follows:

$$\Delta h(x,y) = \begin{cases} h_{p1}, & \left(x-x_{p2}-\frac{a}{2}\right)^2 + (y-y_{p2})^2 \ge {r_{p1}}^2 \,\&\&\, \left(x-x_{p2}+\frac{a}{2}\right)^2 + (y-y_{p2})^2 \le {r_{p2}}^2 \\ h_{p2}, & \frac{b}{2a_1}(x-x_{p2}) - \frac{3b}{4} \le (y-y_{p2}) \le -\frac{b}{2a_2}(x-x_{p2}) + \frac{3b}{4} \,\&\&\, -\frac{b}{2a_2}(x-x_{p2}) - \frac{3b}{4} \le (y-y_{p2}) \\ & \ldots \le \frac{b}{2a_2}(x-x_{p2}) + \frac{3b}{4} \,\&\&\, \frac{b}{2a_3}(x-x_{p2}) - \frac{3b}{4} \le (y-y_{p2}) \le -\frac{b}{2a_3}(x-x_{p2}) + \frac{3b}{4} \end{cases} \tag{3}$$

In general, it is difficult to analyze the unsteady random distribution of asperities on the real contact rough surfaces of mechanical parts, at the locations where the contact of asperity may occur. Based on the self-similarity, the W-M type function in the form of Gaussian distribution is used to characterize the roughness of the bearing and the textured surface (Fang, 2019). In order to apply the W-M type function to the bearing calculation, the reference (Zhang et al, 2016) expands two-dimensional surface roughness $Z(x)$ to three-dimensional surface roughness $Z(x, y)$.

$$z(x,y)=\sum_{m=1}^{\infty} G_m\gamma^{-(3-D_s)n}\sin[\gamma^m(x\cos B_m+y\sin B_m)+A_m] \quad (4)$$

Where G_m is the random number that obeys the normal distribution with a mean of 0 and a variance of 1, that is, the scale coefficient; A_m and B_m are the independent random numbers that obey a uniform distribution on [0, 2π], D_s is the theoretical classification dimension, $D_s\in(2,3)$, γ is a constant greater than 1, usually 1.5, m is the number of natural sequences.

For the composite micro-textured bearings, substituting equation (4) into the equation (1), the oil film thickness equation in the textured region considering surface roughness is as following:

$$\begin{cases} h_3(x,y)=c_r+e\cos(\varphi-\theta)+\Delta h(x,y) \\ h_4(x,y)=c_r+e\cos(\varphi-\theta)+\Delta h(x,y)+z(x,y) \end{cases} \quad (5)$$

Where $h_3(x, y)$ and $h_4(x, y)$ are the oil film thickness equations in the textured region ignoring and considering surface roughness, respectively.

The calculation equation of static characteristic

The lubricant is assumed to be an incompressible, continuous, isotropic Newtonian fluid, and the flow state of the lubricant is assumed to the laminar flow, inertial forces is ignored compared to viscous forces and the pressure distribution of the bearing is described by the classical Reynolds equation (Zhang et al, 1986):

$$\begin{cases} \frac{\partial}{\partial x}\left(h_3^3\frac{\partial p_h}{\partial x}\right)+\frac{\partial}{\partial y}\left(h_3^3\frac{\partial p_h}{\partial y}\right)=6\mu U\frac{\partial h_3}{\partial x} \\ \frac{\partial}{\partial x}\left(h_4^3\frac{\partial p_h}{\partial x}\right)+\frac{\partial}{\partial y}\left(h_4^3\frac{\partial p_h}{\partial y}\right)=6\mu U\frac{\partial h_4}{\partial x} \end{cases} \quad (6)$$

Where p_h is the oil film pressure, μ is the lubricating oil viscosity, U is the journal speed.

For solving the equation (6), the Reynolds boundary conditions are used, the pressure is 0 when pressure is less than 0:

Pressure at the starting point is as following:$p_h=0|_{\varphi=\theta}$,

Pressure at the end point is as following: $p_h=0|_{\varphi=\theta}\&\&\left.\frac{\partial p_h}{\partial \varphi}\right|_{\varphi=\varphi_0}=0$,where φ_0 is the angle at the position of oil film rupture.

Governing equation of dynamic characteristics

As shown in Fig.1, the oil film is approximately regarded as the linearized spring and damping system, the dynamic characteristics of the oil film reflect the change of oil film pressure, when the journal deviates from the static equilibrium position and moves at the position. For the incompressible fluids, the Reynolds equation(Zhang et al, 1986) is as following:

$$\begin{cases} \frac{1}{r^2}\frac{\partial}{\partial\varphi}\left(\frac{{h_3}^3}{12\eta}\frac{\partial p_h}{\partial\varphi}\right)+\frac{\partial}{\partial y}\left(\frac{{h_3}^3}{12\eta}\frac{\partial p_h}{\partial y}\right)=\frac{U}{2r}\frac{\partial h_3}{\partial\varphi}+V_e\cos\varphi+V_\theta\sin\varphi=\frac{U}{2r}\frac{\partial h_3}{\partial\varphi}+\dot{e}\cos\varphi+e\dot{\theta}\sin\varphi \\ \frac{1}{r^2}\frac{\partial}{\partial\varphi}\left(\frac{{h_4}^3}{12\eta}\frac{\partial p_h}{\partial\varphi}\right)+\frac{\partial}{\partial y}\left(\frac{{h_4}^3}{12\eta}\frac{\partial p_h}{\partial y}\right)=\frac{U}{2r}\frac{\partial h_4}{\partial\varphi}+V_e\cos\varphi+V_\theta\sin\varphi=\frac{U}{2r}\frac{\partial h_4}{\partial\varphi}+\dot{e}\cos\varphi+e\dot{\theta}\sin\varphi \end{cases} \quad (7)$$

Where V_e is the speed in the direction of eccentricity, and V_θ is the rotational speed of the axis center around the bearing center.

Therefore, under the normal working conditions, p_h expands into the Taylor series for the instantaneous displacement ($\Delta e=e-e_0$, $e\Delta\theta=e(\theta-\theta_0)$) and the axis displacement velocity $(\dot{e}, e\dot{\theta})$ of the axis static equilibrium position. Since the axis only makes a small displacement at the steady-state position, minor terms above the second order are ignored, the equation can be simplified as:

$$p_h=p_0+p_e\Delta e+p_\theta e\Delta\theta+p_{\dot{e}}+p_{\dot{\theta}}e\dot{\theta} \quad (8)$$

Where $p_0=p_h(\varphi, y, e_0, \theta_0, 0, 0)$, p_e, p_θ, $p_{\dot{e}}$, $p_{\dot{\theta}}$ are the disturbance pressure, $p_e=\left(\frac{\partial p_h}{\partial e}\right)_0$, $p_\theta=\left(\frac{1}{e}\frac{\partial p_h}{\partial\theta}\right)_0$, $p_{\dot{e}}=\left(\frac{\partial p_h}{\partial\dot{e}}\right)_0$, $p_{\dot{\theta}}=\left(\frac{1}{e}\frac{\partial p_h}{\partial\dot{\theta}}\right)_0$, the subscript of 0 means to the derivative at the steady state position.

Integrating the equation (8), the oil film force equation (9) can be obtained when the bearing is subjected to a small displacement, and expanding f_e and f_θ into Taylor series near the steady-state position and retaining the linear term, the equation (10) can be obtained:

$$\begin{Bmatrix} f_e \\ f_\theta \end{Bmatrix}=-\int_0^l\int_{\varphi_1}^{\varphi_2} p_h\begin{Bmatrix}\cos\varphi \\ \sin\varphi\end{Bmatrix}rd\varphi dy \quad (9)$$

$$\begin{Bmatrix} f_e \\ f_\theta \end{Bmatrix}=\begin{cases} f_{e_0}+\left(\frac{\partial f_e}{\partial e}\right)_0\Delta e+\left(\frac{\partial f_e}{e\partial\theta}\right)_0 e\Delta\theta+\left(\frac{\partial f_e}{\partial\dot{e}}\right)_0\dot{e}+\left(\frac{\partial f_e}{e\partial\dot{\theta}}\right)_0 e\dot{\theta} \\ f_{\theta_0}+\left(\frac{\partial f_\theta}{\partial e}\right)_0\Delta e+\left(\frac{\partial f_\theta}{e\partial\theta}\right)_0 e\Delta\theta+\left(\frac{\partial f_\theta}{\partial\dot{e}}\right)_0\dot{e}+\left(\frac{\partial f_\theta}{e\partial\dot{\theta}}\right)_0 e\dot{\theta} \end{cases} \quad (10)$$

Introducing $k_{ee}=\left(\frac{\partial f_e}{\partial e}\right)_0$, $k_{e\theta}=\left(\frac{\partial f_e}{e\partial\theta}\right)_0$, $k_{\theta e}=\left(\frac{\partial f_\theta}{\partial e}\right)_0$, $k_{\theta\theta}=\left(\frac{\partial f_\theta}{e\partial\theta}\right)_0$, there are four derivatives of the oil film force to the axial displacement, which is called the stiffness coefficient, and is represented by k_{ij}, i is the direction of force increment, and j is the direction of position increment; $b_{ee}=\left(\frac{\partial f_e}{\partial\dot{e}}\right)_0$, $b_{e\theta}=$

$\left(\frac{\partial f_e}{e\partial\dot{\theta}}\right)_0$, $b_{\theta e}=\left(\frac{\partial f_\theta}{\partial \dot{e}}\right)_0$, $b_{\theta\theta}=\left(\frac{\partial f_\theta}{e\partial\dot{\theta}}\right)_0$, which is the derivative of the oil film force to the displacement speed of the bearing axis, it is called the oil film damping coefficient, and it is represented by b_{ij}.

In order to easily evaluate the stability of the bearing rotor, it is necessary to convert the coordinate (e,θ) into the Cartesian coordinate system. Since the coordinate system (e,θ) is an angle ahead of the Cartesian coordinate system, the dynamic coefficient in the Cartesian coordinate system can be expressed as follows:

$$\begin{bmatrix}K_{xx} & K_{xy}\\ K_{yx} & K_{yy}\end{bmatrix}= \begin{bmatrix}\sin\theta & \cos\theta\\ \cos\theta & -\sin\theta\end{bmatrix}\begin{bmatrix}k_{ee} & k_{e\theta}\\ k_{\theta e} & k_{\theta\theta}\end{bmatrix}\begin{bmatrix}\sin\theta & \cos\theta\\ \cos\theta & -\sin\theta\end{bmatrix} \quad (11)$$

$$\begin{bmatrix}B_{xx} & B_{xy}\\ B_{yx} & B_{yy}\end{bmatrix}= \begin{bmatrix}\sin\theta & \cos\theta\\ \cos\theta & -\sin\theta\end{bmatrix}\begin{bmatrix}b_{ee} & b_{e\theta}\\ b_{\theta e} & b_{\theta\theta}\end{bmatrix}\begin{bmatrix}\sin\theta & \cos\theta\\ \cos\theta & -\sin\theta\end{bmatrix} \quad (12)$$

Numerical Solving

The computed bearing parameters and working conditions are shown in Table 1 according to our previous study (Zhao, 2020) and (Wang et al, 2024). The micro-texture is located on the surface of the bearing pad, the texture starting angle of the circumferential distribution is φ_1=45°and the texture in the axial direction is fully covered. Taking the rectangular texture as an example, the texture size is $a\times b$=400μm×400μm, and the texture density is 10%, texture depth is 9μm, and the circular micro-texture ensures the same area and the same depth. Oil film thickness equation (5) and Reynolds equation (6), (7) are computed by the finite difference method, journal bearing pressure and dynamic characteristics coefficient are obtained. When calculating the static characteristics using equation (5), (6), carrying capacity should satisfy that the ratio of bearing capacity in the x direction to that in the y direction is less than 4×10^{-3}. After solving the static characteristics, the equation (7)-(10) are solved, Reynolds boundary condition is used, the pressure and disturbance pressure distribution of oil film can be obtained, by integrating the journal bearing disturbance pressure using the Simpson method and coordinate transformation equation (11), (12), the stiffness coefficient and damping coefficient can be obtained.

Table 1 Parameters of micro-texture journal bearing

Parameter	Symbol	Numerical value
Bearing radius /mm	R	15
Radius clearance /μm	c_r	30
Environmental pressure /Pa	P_{air}	1×10^5
Journal speed /(r • min^{-1})	n	6000
Lubricating oil viscosity /(Pa·s)	μ	0.0035

The journal bearing is the basis of the analysis and calculation of the micro-textured journal bearing, in order to ensure the calculation correctness, it is necessary to verify the calculation results of the theoretical model of the journal bearing. Using the parameters from reference (Tala-Ighil et al, 2011), by comparison with the reference in Table 2, it can be obtained that the error between the calculation results of the manuscript and the reference is within 10%.

Table 2 Calculation in reference (Tala-Ighil et al, 2011) and the manuscript

Grid numbers	Results	Eccentricity	Minimum oil film thickness	Maximum pressure
297×48	Reference	0.6012	11.9647	7.7075
	Computed results	0.6458	10.4968	8.0987
	Error	7.418%	12.26%	5.075%
594×95	Reference	0.6018	11.9456	7.7321
	Computed results	0.6232	11.2973	7.8659
	Error	3.55%	5.42%	1.73%

Using the parameters from reference (Zhang et al, 2016), compared with the reference, it is the asperity rough surface that satisfies the Gaussian distribution, and as shown in Table 3, compared with the numerical and theoretical results of the reference, the errors calculated in the manuscript are all within 10% and the numerical values are relatively close.

Table 3 Comparison of the calculation results with the reference (Zhang et al, 2016)

	Average value (μm)	Root mean square deviation (μm)	Kurtosis
Theoretical value	0	0.5	3
Reference	0.0032	0.5015	3.0406
Calculation results	0.0046	0.5039	3.0664

Numerous studies have shown that the bearing roughness is between 0.2 μm and 0.8 μm. The rough surface with the mean value of about 0 and a root mean square deviation of about 0.21 μm is used to study the lubricating performance of the rough surface composite textured bearing.

RESULTS AND ANALYSIS

The effect of roughness on bearing lubrication performance

Many studies have shown that the size of roughness will affect the lubrication performance of bearings, but the research on the size of composite texture bearing roughness is still relatively less, and there is no unified conclusion. Figure 3 show the oil film thickness of non-textured bearings and circular composite rectangular under different roughness. As shown in Figure 3, as the roughness of the bearing

increases, the surface of oil film becomes more and more rough, and as the roughness increases, the minimum of the oil film thickness gradually decreases. In Figure 4, as the roughness of bearing increases, oil film pressure fluctuates more and more, oil rupture location delays, maximum pressure of oil film increases first and then decreases with the increase of roughness. Maximum pressure is obtained when the roughness of smooth bearing is 0.303μm, and maximum pressure is obtained when the roughness of composite bearing is 0.209μm because the texture influences the oil film thickness, but the presence of texture has little effect on oil film rupture location.

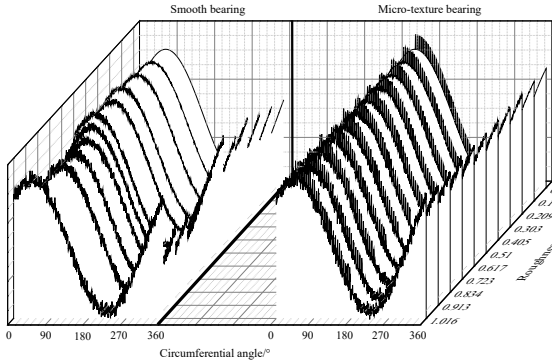

Fig.3 Oil film thickness under different roughness

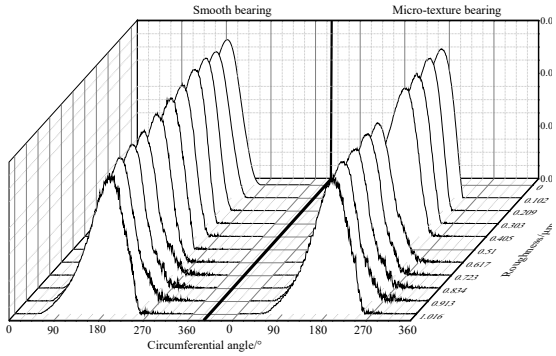

Fig.4 Oil film pressure under different roughness

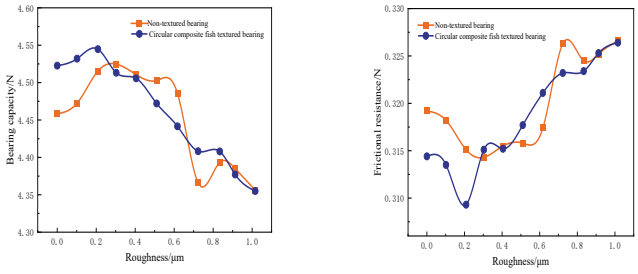

(a) Bearing capacity (b) Friction coefficient

Fig.5 Loading capacity and friction coefficient under different roughness

Figure 5 shows the bearing capacity and friction coefficient of the circular composite rectangular textured bearing and the non-textured bearing under different roughness. As shown in Fig. 5(a), the bearing capacity of the composite textured bearing and the non-textured bearing first increases and then decreases with the increase of roughness. When the roughness is 0.209μm, the bearing capacity of the composite textured bearing is the largest, which is 1.94% higher than that of the non-textured surface bearing; the bearing capacity of the non-textured bearing is the largest when the roughness is 0.303μm, which is 1.61% higher than that of the bearing without considering roughness. In addition, when the roughness of the composite textured bearing exceeds 0.209 μm, the bearing capacity of the composite textured bearing is gradually lower than that of the non-textured bearing. Figure 5(b) is the friction coefficient diagram of the non-textured bearing and the composite textured bearing. It can be found that the variation trend of the friction coefficient is opposite to that of the bearing capacity, and decreases first and then increases with the increase of roughness. When the roughness of the composite textured bearing is 0.209 μm, the friction coefficient is the smallest, which is 3.11% lower than that of the non-textured bearing; when the roughness of the non-textured bearing is 0.0303 μm, the friction coefficient is the smallest, which is 1.54% lower than that when the roughness is not considered.

Influence of different texture distribution positions considering roughness on bearing performance

Figure 6 shows the bearing capacity and friction resistance of circular composite crescent texture at different termination angles. As shown in Figure 6, the bearing capacity and the change trend of friction force with the termination angle considering the roughness are the same as those of composite textured bearings without considering the roughness. The bearing capacity first increases and then decreases with the increase of the termination angle, and the friction resistance first decreases and then increases with the increase of the termination angle. The corresponding positions of the maximum bearing capacity and the minimum friction resistance are the same, are both at the termination angle of 160°.

In addition, when the termination angle is small, the bearing performance considering roughness will increase more, the bearing capacity will increase the most, and the friction resistance will decrease the most; with the increase of the termination angle, the curve considering the roughness is closer and closer to the corresponding curve without considering the roughness, and the difference of bearing performance is smaller and smaller. The reasons for the phenomenon are as following: when the termination angle is small, the texture region is small, and the non-texture region is large, the roughness has an obvious effect on the characteristics of the bearing, there is a large gap between the composite texture bearing considering the roughness and ignoring the roughness. With the increase of the termination angle, the texture region becomes larger, the number of textures becomes more, the increase effect of texture on the bearing increases, while the increase effect of

roughness on the bearing is gradually not obvious, at the time, the performance of bearing considering roughness is closer to that of bearing without considering roughness.

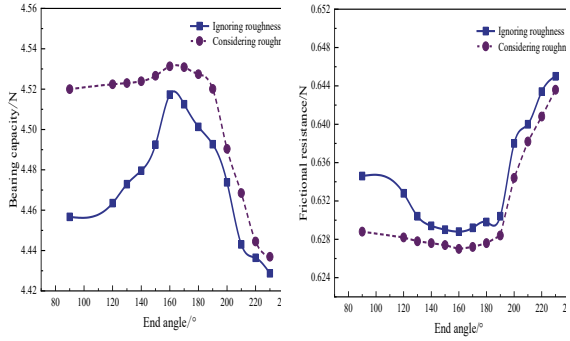

(a) Bearing capacity at different termination angles

(b) Bearing friction resistance at different termination angles

Fig.6 Static characteristics of compound textured journal bearing under different termination angles

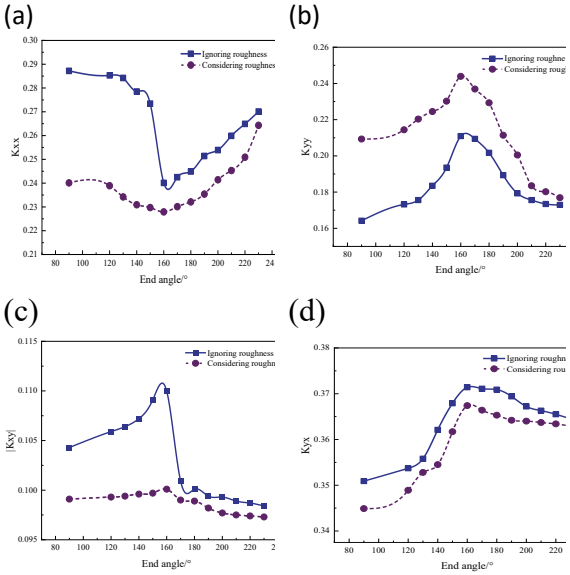

Fig.7 Dimensionless stiffness coefficient of compound textured journal bearing at different termination angles: (a) K_{xx} (b) $|K_{xy}|$ (c) K_{yx} (d) K_{yy}

Figure 7 shows the stiffness coefficients of composite textured bearings without considering roughness and considering roughness at different termination angles. The change trend of stiffness coefficient of composite texture bearing considering roughness with termination angle is consistent with that of composite texture bearing without considering roughness, both of which reach the optimal value near the termination angle of 160°; the direct stiffness coefficient K_{yy} considering the roughness is 15.6% higher than that without considering the roughness, and the cross coupling stiffness coefficients $|K_{xy}|$ considering the roughness are 9% lower than that without considering the roughness. which shows that the composite texture considering the roughness has the strongest resistance to the external force in the y direction when termination angle is 160 °, and the input whirling energy is the smallest, lubrication performance is better. With the increase of the termination angle, the stiffness coefficients considering roughness and ignoring roughness are getting closer and closer, which shows that the influence of roughness on bearing performance is weakened, which is consistent with the conclusion obtained in Fig.6.

Figure 8 shows the damping coefficient of composite texture bearing without considering roughness and considering roughness at different termination angles. The damping coefficient of composite texture bearing considering roughness is the same as that of bearing without considering roughness, which decreases first and then increases with the end angle of texture, the minimum value is taken at the end angle of 160 °, B_{yy} decreases by 17.72%, and B_{yx} and B_{xy} decrease by 2.3%, compared with that without considering roughness. With the increase of the termination angle, the damping coefficient considering roughness is closer to that without considering roughness, which is consistent with the change trend of Fig.6 and Fig.7, indicating that the influence of roughness on the bearing becomes smaller.

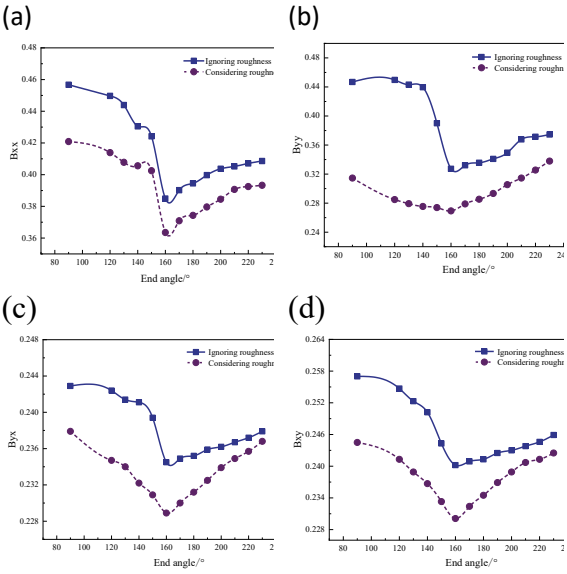

Fig.8 Dimensionless damping coefficient of compound micro textured journal bearing at different termination angles: (a) B_{xx} (b) B_{yy} (c)B_{xy} (d)B_{yx}

Therefore, the bearing performance considering roughness first increases and then decreases with the increase of termination angle, which is consistent with the change trend of the bearing without considering roughness, and the bearing performance is the best the end angle of 160°. Compared with the texture bearing without considering the roughness, the roughness can enable the bearing to obtain greater bearing capacity and K_{yy}, smaller friction resistance, cross stiffness coefficient and damping coefficient, and better bearing performance. The effect of roughness on

bearing performance decreases with the increase of texture termination angle.

Influence of different arrangements of composite micro textures on bearing performance

As shown in Fig. 2 and Fig.9, the same texture arranges along the circumferential motion direction, and the textures of different shapes arrange along the axial direction, so that the circumferential corresponding parallel arrangement of Fig. 2 is obtained. Rotating the texture arrangement of Fig.2 by 90°, the texture of the same shape arranges along the axial direction, and the texture of different shapes arranges along circumferential direction, the axial corresponding parallel arrangement of Fig. 9 is obtained. The circumferential staggered parallel arrangement and axial staggered parallel arrangement

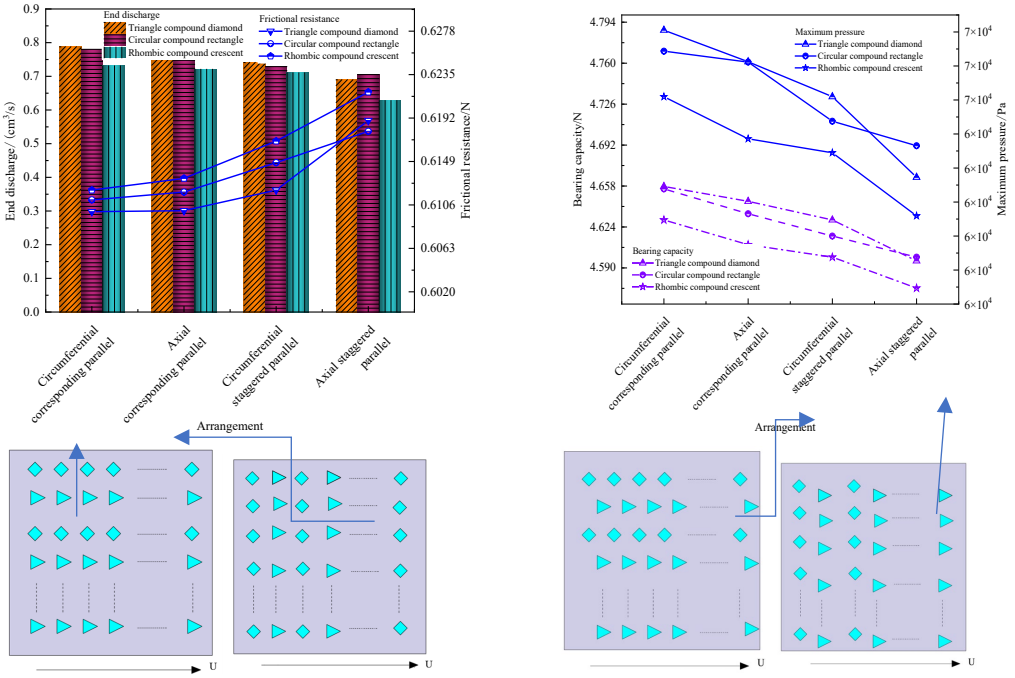

(a) End leakage, frictional resistance (b) Carrying capacity, maximum pressure

Fig. 9 Bearings static characteristics of different arrangements considering the surface roughness

of Fig. 9 can be obtained by interlacing the textures along the circumferential and axial directions respectively.

As shown in Fig. 9, considering the surface roughness, the bearing capacity of composite micro texture bearings, maximum pressure, end leakage reduces in the order of circumferential corresponding arrangement, axial corresponding arrangement, circumferential staggered arrangement and axial staggered arrangement, while the friction coefficient gradually increases. The static characteristics of circumferential corresponding parallel arrangement is best. When the arrangement is circumferential corresponding arrangement, the same shape texture is parallel to the direction of motion, which is conducive to reducing the outflow of lubricating oil from the bearing wedge space and enhancing the hydrodynamic effect of bearing; each micro-texture distributes in the pressure rise region will cause that the inflow of lubricating oil is greater than the outflow, greater hydrodynamic effect is obtained.

And in Fig.9, the triangular composite diamond texture has better static characteristics, and the diamond composite crescent has worse static characteristics, which is because that the gradual convergence of triangle and diamond structures along the direction of motion, produces the stronger hydrodynamic effect and is more conducive to improving the static characteristics of bearings.

As shown in Fig. 10 (a) and (b), the bearing oil film stiffness coefficient K_{yy} considering the roughness is higher than that ignoring the roughness, K_{xx} considering the roughness is smaller than that ignoring the roughness. The K_{yy} of the circular composite rectangle in the circumference corresponding parallel arrangement considering the roughness increases by 8.79% compared with ignoring roughness, which means that the stability of the bearing is stronger after considering the roughness. It can be seen from the Fig. 10(b) that the stiffness coefficient K_{yy} of bearing in different arrangements is greater than that of non-textured bearings, which means that machining the composite textures in different arrangements on the bearing surface will improve the stiffness coefficient K_{yy} of bearings, and improve the bearing's ability to resist the external forces from the y direction. For the K_{yy} in the circumferential corresponding parallel arrangement is the largest, and the axial staggered parallel arrangement is the worst, which means that the circumferential corresponding parallel arrangement

can obtain a greater direct stiffness coefficient K_{yy}, and the stability of the bearing is stronger.

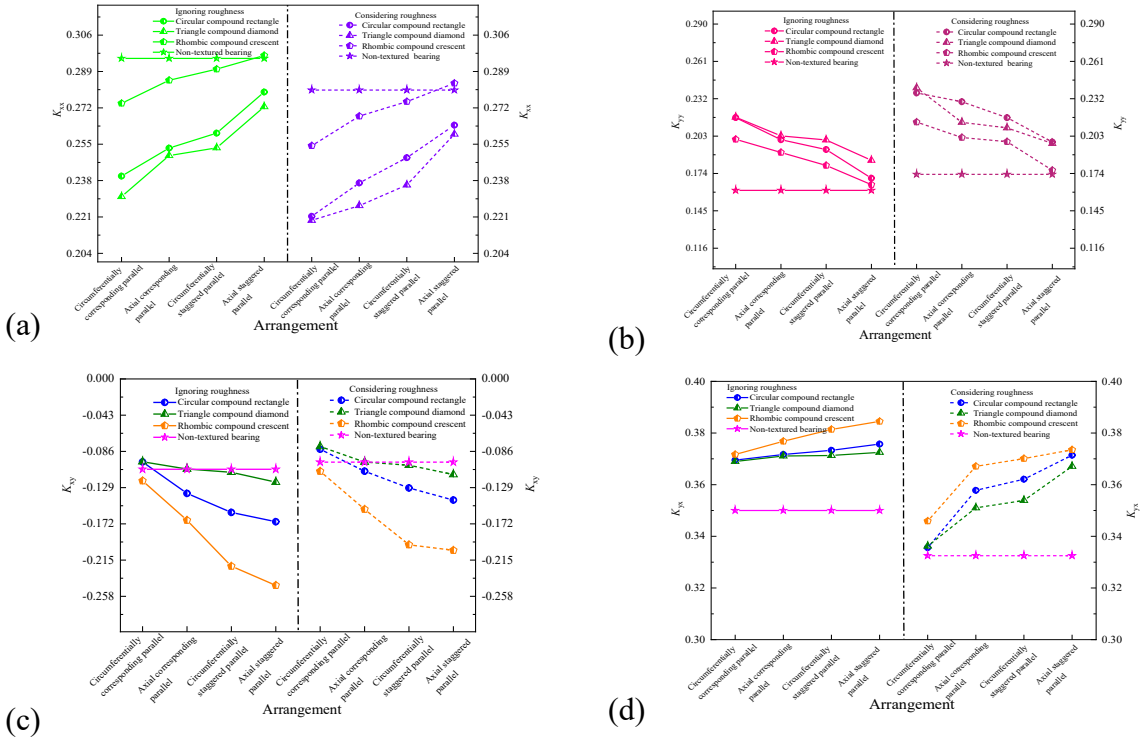

Fig. 10 Effect of roughness on the stiffness coefficient of composite micro texture bearing under different arrangement modes (a) K_{xx} (b)K_{yy} (c) K_{xy} (d)K_{yx}

As shown in Fig. 10 (c) and (d), $|K_{xy}|$ and K_{yx} of bearing decrease after considering the roughness, taking the circular composite rectangular bearing in the circumferential corresponding parallel arrangement as an example, $|K_{xy}|$ and K_{yx} decrease by 17.99% and 6.39% considering the upper roughness, which indicates that the whirl energy input by the bearing oil film is less and the bearing is more stable considering the upper roughness; it can also be seen that the $|K_{xy}|$ and K_{yx} in the circumferential corresponding parallel arrangement are the minimum, and the axial staggered parallel arrangement is the maximum.

The triangular composite diamond texture has the largest K_{yy} , and the absolute value of the cross coupling stiffness coefficient is the smallest, which can obtain better stability, which is consistent with the previous study (Wang, 2023) ; the diamond composite crescent has the smallest value of K_{yy}, and the absolute value of cross coupling stiffness coefficient is the largest, which does not improve significantly the stability of bearing. It can be seen from the Figure 11 that the damping coefficient of bearing considering roughness decreases. Taking the circular composite rectangular micro textured bearing in circumferential corresponding parallel arrangement as an example, the direct damping coefficient B_{yy} considering roughness decreases by 5.12%, which shows that the bearing considering roughness obtains less damping. The damping coefficient of oil film for various composite micro texture bearings with different arrangements is smaller than that of non-textured bearings, and the damping coefficients of the circumferential corresponding arrangement is the smallest. For the direct damping coefficient B_{yy} considering roughness, the triangular composite diamond in the circumferential corresponding arrangement is 32.82% lower than the non-textured bearing, and the diamond composite crescent bearing is 29.12% lower than the non-textured bearing. For the damping coefficient B_{xx}, the triangular composite diamond in the circumferential corresponding parallel arrangement is 17.77% lower than the non-textured bearing, and the diamond composite crescent bearing is 11.84% lower than the non-textured bearing. For the cross coupling damping coefficients B_{xy} and B_{yx} of bearings, three composite micro textured bearings with circumferential corresponding parallel arrangement decrease the most than non-textured bearings. Therefore, the circumferential corresponding parallel arrangement with appropriate roughness should be selected to process the composite micro texture arrangement to obtain less bearing damping.

By analyzing the stiffness and damping of different composite textures, the texture arrangement composed of different texture shapes have different effect on the improvement of bearing performance. The damping coefficient of triangular composite diamond texture is the smallest, and K_{yy} is the largest, and the cross coupling stiffness coefficient is the

smallest, which is more conducive to improving the dynamic characteristics of the bearing; the rhombic compound crescent has the least improvement on the dynamic characteristics of bearing. It is consistent with the results of static characteristics.

Combined with the results of static and dynamic characteristics, when considering the roughness, composite texture bearings in the circumferential corresponding parallel arrangement have larger bearing capacity, smaller friction coefficient, larger K_{yy}, smaller cross coupling stiffness coefficient, smaller damping coefficient, and have better tribological performance.

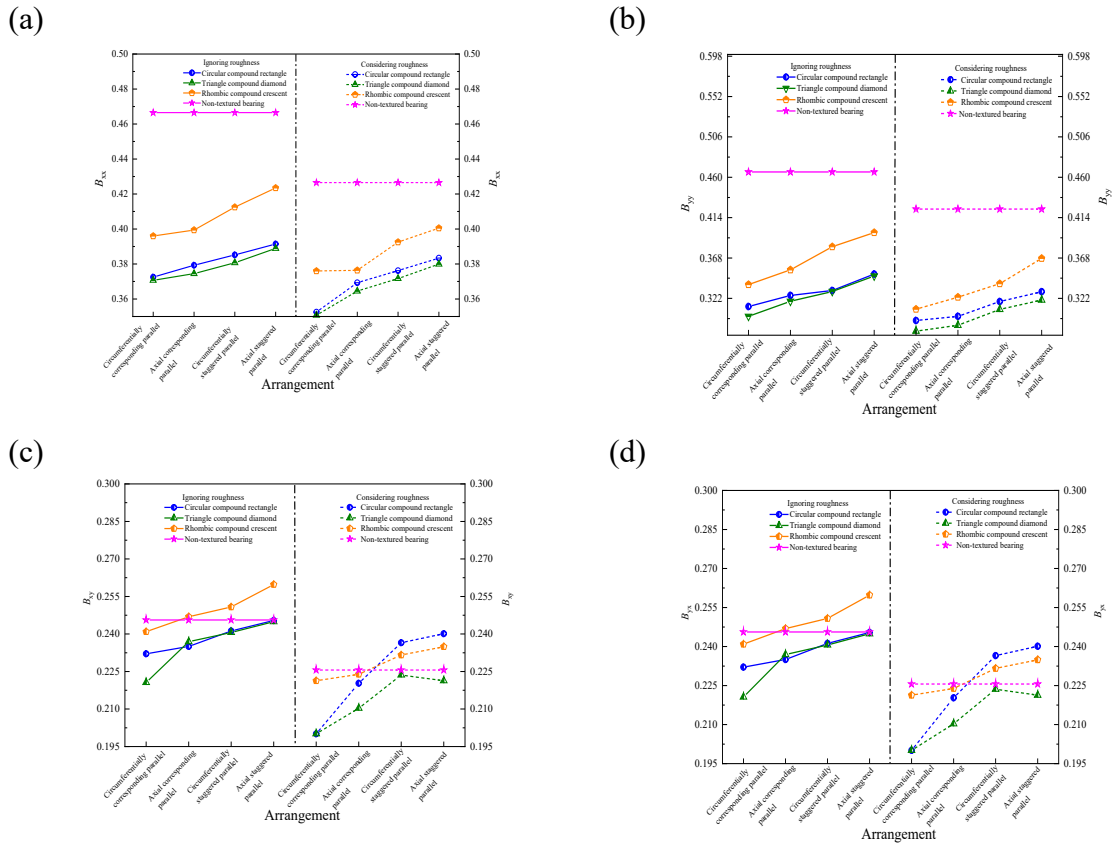

Figure 11 Dimensionless damping coefficient of composite micro textured bearing considering roughness in different arrangements: (a)B_{xx} (b)B_{yy} (c)B_{xy} (d)B_{yx}

CONCLUSIONS

To improve the static and dynamic characteristics of journal bearings, the surface roughness model, the oil film thickness equation of composite micro texture, the generalized Reynolds equation of journal bearings, and the dynamic characteristics calculation model of bearing rotor system are established. The static and dynamic characteristics of bearings with different distribution positions and arrangements of composite micro texture considering the roughness are studied.

The proper roughness of the contact surface is more conducive to enhancing the hydrodynamic effect of the bearing and improving the stability of the bearing. The friction coefficient of composite textured bearing is the lowest when the roughness is 0.209μm. The optimal roughness of composite micro-textured journal bearing is smaller than that of the smooth bearing, composite textured bearings require higher machining accuracy.

The bearing performance considering roughness first increases and then decreases with the increase of termination angle, and the bearing performance is best at 160°. The effect of roughness on bearing performance decreases with the increase of texture termination angle.

The arrangement of micro-textures will affect the performance of the bearing. When the micro-textures are arranged in the circumferentially corresponding parallel arrangement, it has better hydrodynamic characteristics. The shape of the micro-texture will also affect the bearing performance. The triangular composite diamond has the largest bearing capacity and the smallest friction resistance; considering the roughness, K_{yy} is the largest, the $|K_{xy}|$ and K_{yx} are the smallest, the damping coefficient is smaller for the triangular composite diamond. Therefore, the triangular composite diamond bearing with circumferential corresponding parallel arrangement

can obtain better static and dynamic characteristics of the bearing, which is the most obvious to improve the tribological performance of bearing.

ACKNOWLEDGEMENTS

This work was supported by Shandong Province Key Laboratory of Mine Mechanical Engineering, Shandong University of Science and Technology (2022KLMM304), Qingdao Postdoctoral Research funded project.

REFERENCES

Atwal, J.C., Pandey, R.K.(2021). Performance analysis of thrust pad bearing using micro-rectangular pocket and bionic texture. Proceedings of the Institution of Mechanical Engineers, Part J: *Journal of Engineering Tribology*, 235(6):1232-1250. https://doi.org/10.1177/1350650120940076

Chang, J., Cai, W.(2013). Chaotic response and bifurcation analysis of rotor-bearing system with nonlinear suspension and roughness effect under turbulent flow. *Smart Science*, 1(1): 41-50. https://doi.org/10.1080/23080477.2013.11665585

Chen, P, Liu, J.Y., Hong, J.Z.(2018). Simulation and experimental investigation on the eccentric collision in multi-body systems considering the friction effect. *Journal of Vibration and Shock*, 37(1): 1-7. https://doi.org/10.13465/j.cnki.jvs.2018.01.001

Cheng, J, Gu, C. X. (2024). Effects of surface morphology on the performance of water-lubricated thrust bearings. Industrial Lubrication and Tribology, 76(3): 337-344. https://doi.org/ 10.1108/ILT-08-2023-0247

Dobrica, M. B., Fillon, M (2009). About the validity of Reynolds equation and inertia effects in textured sliders of infinite width. *Proceedings of the Institution of Mechanical Engineers, Part J: Journal of Engineering Tribology*, 223(1): 69-78.

Fang, C.(2019). Analysis of dynamic response characteristics of contact interface with microtexture. Shenyang: Shenyang Jianzhu University.

Gururajan, K., Prakash, J.(2000). Effect of Surface Roughness in a Narrow Porous Journal Bearing. *Journal of Tribology*. 122(2):472-475. https://doi.org/10.1115/1.555387

Hua, X.J., Tian, Z.X., Xie, X., et al.(2020).Tribological Behavior and Abrasion Resistance Mechanism of Laser Micro-Bulge Texturing Surface under Full Oil Lubrication. *Tribology Transactions*, 63(4): 726-735. https://doi.org/10.1080/10402004.2020.1738610

Huang, Q.P., Shi, X.L., Xue, Y.W., et al.(2022). Wear-triggered self-repairing behavior of bionic textured AISI 4140 steel filled with multi-solid lubricants. *Wear*,204416. https://doi.org/10.1016/j.wear.2022.204416

Kumar, V., Sharma, S.C.(2019). Effect of geometric shape of micro-grooves on the performance of textured hybrid thrust pad bearing. *Journal of the Brazilian Society of Mechanical Sciences and Engineering*, 41(11): 508. https://doi.org/10.1007/s40430-019-2016-0

Kumarab, R., Azama, M. S.(2021). Effect of directionally oriented random roughness on performance of a Rayleigh step bearing operating under Mixed-Elastohydrodynamic Lubrication. *Tribology International*,106572. https://doi.org/10.1016/j.triboint.2020.106572

Li, S.S., An, Q.(2019). Lubrication performance of planar thrust bearing with consideration of roughness of the surfaces. Proceedings of the Institution of Mechanical Engineers, Part J: *Journal of Engineering Tribology*, 233(7): 1046-1058. https://doi.org/10.1177/1350650118813818

Maharshi. K., Mukhopadhyay, T., Roy, B., Roy, L., Dey, S.(2018). Stochastic dynamic behaviour of hydrodynamic journal bearings including the effect of surface roughness. *International Journal of Mechanical Sc-iences*, 370-383. https://doi.org/10.1016/j.ijmecsci.2018.04.012

Manser, B., Belaidi, I., Khelladi, S., et al.(2020). Computational investigation on the performance of hydrodynamic micro-textured journal bearing lubricated with micropolar fluid using mass-conserving numerical approach. Proceedings of the Institution of Mechanical Engineers, Part J: *Journal of Engineering Tribology*, 234(8):1310-1331. https://doi.org/10.1177/1350650119894167

Meng, Y., Deng, J.X., Zhang, Y., et al.(2020). Tribological properties of textured surfaces fabricated on AISI 1045 steels by ultrasonic surface rolling under dry reciprocating sliding. *Wear*, 203488. https://doi.org/10.1016/j.wear.2020.203488

Narwat Kuldeep, Kumar Vivek, Singh Simran Jeet, Kumar Abhishek, Sharma Satish C. (2023). Performance of rough surface hydrodynamic circular and multi-lobe journal bearings in turbulent regimes.Proceedings of the Institution of Mechanical Engineers, Part J: Journal of Engineering Tribology, 237(4): 860-880.

https://doi.org/10.1177/13506501221117956

Niu, Y.X., Pang, X.J., Yue, S.W. et al. (2021). The friction and wear behavior of laser textured surfaces in non-conformal contact under starved lubrication. *Wear*, 203723. https://doi.org/10.1016/j.wear.2021.203723

Obilor, A.F., Pacella, M., Wilson, A., et al.(2022). Micro-texturing of polymer surfaces using lasers: a review. *The International Journal of Advanced Manufacturing Technology*, 120(1-2):103-135. https://doi.org/10.1007/s00170-022-08731-1

Pattnayak, M. R., Pandey, R. K., Dutt, J. K.(2022). Performance Improvement of an Oil-Lubricated Journal Bearing Using Bionic-Textures Fused Micro-Pockets. *Journal of Tribology*, 144(4):041804. https://doi.org/10.1115/1.4051654

Profito, F.J, Vladescu, S.C., Reddyhoff, T., Dini,D.(2024). Numerical and experimental investigation of textured journal bearings for friction reduction. Tribology International, 195:109643.

Singh, U. P.(2020). Mathematical analysis of effects of surface roughness on steady performance of hydrostatic thrust bearings lubricated with rabinowitsch type fluids. *Journal of Applied Fluid Mechanics*, 13(4): 1339-1347. https://doi.org/ 10.36884/jafm.13.04.30682

Son, P.B., Molinari, J.F.(2021). Creation and evolution of roughness on silica under unlubricated wear. *Wear*, https://doi.org/203648. 10.1016/j.wear.2021.203648

Tala-Ighil, N., Fillon, M., Maspeyrot, P.(2011). Effect of textured area on the performances of a hydrodynamic journal bearing. *Tribology International*, 44(3): 211-219. https://doi.org/10.1016/j.triboint.2010.10.003

Tauviqirrahman, M., Jamari, J., Muchammad, M., et al.(2022). Hydrodynamic lubrication analysis of hydrophobic textured journal bearing considering cavitation. *Cogent Engineering*, 9(1): 2069997. https://doi.org/10.1080/23311916.2022.2069997

Vidyasagar K. E. Ch, Pandey R. K, Kalyanasundaram Dinesh. (2021). Improvement of Deep Groove Ball Bearing's Performance Using a Bionic Textured Inner Race. Journal of Bionic Engineering.,18(4):974-990. https://doi.org/10.1007/s42235-021-0056-5

Wang, Z.Q., Xiang, J.B., Fu, Q., et al.(2022). Study on the Friction Performance of Textured Surface on Water Hydraulic Motor Piston Pair. *Tribology Transactions*, 65(2): 308-320. https://doi.org/10.1080/10402004.2022.2027589

Wang, H.J., Tian, L.L., Zheng, J., et al.(2022). The synergetic effects of laser texturing and super-hydrophobic coatings on improving wear properties of steel. *Tribology International*, 173: 107657. https://doi.org/10.1016/j.triboint.2022.107657

Wang, L.L., Guo, S.H., Wei, Y.L., et al. (2019).Optimization research on the lubrication characteristics for friction pairs surface of journal bearings with micro texture. *Meccanica*, 54(8): 1135-1148. https://doi.org/10.1007/s11012-019-01015-1

Wang, L. L., Zhang W., Ge X., et al. (2023). Effect of compound micro texture arrangement on journal bearing lubrication performance. *China Surface Engineering*, 36(1): 145-155. https:// doi.org/10. 11933 / j. issn. 1007−9289. 20220502001

Wang, L. L., Zhang W., Duan J. D., et al. (2024). Dynamic characteristics analysis of composite micro textured bearings considering roughness. *Journal of Vibration, Measurement & Diagnosis*, 44(3):544-550,621,622. https://doi.org/ 10.16450/j.cnki.issn.1004-6801.2024.03.017

Zhang, H., Liu, Y., Wang, W., Qin, L.G., Dong, G.N.(2019). Surface texture design and its tribological application. *Journal of Mechanical Engineering*, (17):85-93. https://doi.org/ 10.3901/JME.2019.17.085

Zhang, H., Hua, M., Dong, G.Z., et al.(2016). A mixed lubrication model for studying tribological behaviors of surface texturing. *Tribology International*, 93: 583-592. https://doi.org/ 10.1016/j.triboint.2015.03.027

Zhou, X.X., Peng, X.J., Yue, S.W., Zhang, Y.Y., Zhang, H., Yu, B.(2021). Tribological properties of combination of surface texture and ionic liquids. *Tribology*,(6):995-1003. https://doi.org/10.16078/j.tribology.2021109

Zhao, X.T.(2020). Effect of bionic micro texture on friction and wear properties of journal bearing. Qing dao: Shandong University of Science and Technology.

Zhang, Z., Sun, J., Zhao,J.W., Xu,Z.H.(2017). Review of the lubrication research of sliding bearing considering the surface roughness and elastic deformation. *Journal of Machine Design*, 34(5), 1-5. https://doi.org/ 10.13841/j.cnki.jxsj.2017.05.001

Zhang, Z.M., Zhang, Y.Y., Xie, Y.B., et al.(1986). The hydrodynamic lubrication theory of journal bearing. Beijing: Higher Education Press.

NOMENCLATURE

a the size of the circumferential length

A_m, B_m the independent random numbers

b the size of the directional length

b_{ee}, $b_{e\theta}$, $b_{\theta e}$, $b_{\theta\theta}$ damping coefficient, the oil film force to the displacement speed of the bearing axis

B_{ij} oil film damping coefficient, i is the direction of force increment, j is the direction of position increment

c_r the radial clearance of the journal bearing

D_s the theoretical classification dimension

e the eccentricity

G_m the random number

h_1, h_2 the oil film thickness without considering and considering the micro texture

h_3, h_4 the oil film thickness equations in the textured region ignoring and considering surface roughness

h_{max} maximum oil film thickness

k_{ee}, $k_{e\theta}$, $k_{\theta e}$, $k_{\theta\theta}$ stiffness coefficient, four derivatives of the oil film force to the axial displacement

K_{ij} stiffness coefficient, i is the direction of force increment, j is the direction of position increment

m the number of natural sequences

n rotational speed

p the circumferential texture number

p_h the oil film pressure

r_p the radius of the micro-texture

r, R axis and bearing radius

U the journal speed

p_e, p_θ, $p_{\dot{e}}$, $p_{\dot{\theta}}$ the disturbance pressure

q the axial texture number

V_e, V_θ the speed in the direction of eccentricity, the axis center around the bearing center

x, y the circumferential and axial coordinate

Z surface roughness value

φ the circumferential angle

φ_0 the angle at the position of oil film rupture

φ_1, φ_2 the start angle and end angle of micro-textured regions

λ the axial direction of the journal bearing

θ the attitude angle

γ a constant

Δh the texture depth

Δe, $e\Delta\theta$ the instantaneous displacement of the axis static equilibrium position

$\dot{e}$, $e\dot{\theta}$ the axis displacement velocity of the axis static equilibrium position

μ the lubricating oil viscosity